Hindawi Publishing Corporation
Advances in Materials Science and Engineering
Volume 2014, Article ID 273632, 6 pages
http://dx.doi.org/10.1155/2014/273632

Research Article

Evidence of a Lead Metathesis Product from Calcium Hydroxyapatite Dissolution in Lead Nitrate Solution

Oratai Saisa-ard,[1] Weenawan Somphon,[2] Winya Dungkaew,[3] and Kenneth J. Haller[3]

[1] *Chemistry Program, Faculty of Science, Ubon Ratchathani Rajabhat University, Ubon Ratchathani 34000, Thailand*
[2] *Chemistry Department, Faculty of Liberal Arts and Science, Kasetsart University Kamphaeng Saen Campus, Nakhon Pathom 73140, Thailand*
[3] *School of Chemistry, Institute of Science, Suranaree University of Technology, Nakhon Ratchasima 30000, Thailand*

Correspondence should be addressed to Oratai Saisa-ard; oratai_phasai@yahoo.com and Kenneth J. Haller; ken.haller@gmail.com

Received 31 May 2013; Revised 8 November 2013; Accepted 19 November 2013; Published 3 February 2014

Academic Editor: Gomaa El-Damrawi

Calcium hydroxyapatite, CaHAp, synthesized by the precipitation method, was utilized to study the calcium-lead metathesis reaction on dissolution in a lead nitrate solution under reflux conditions to prepare larger lead hydroxyapatite, PbHAp, crystals from CaHAp. SEM images show development of crystalline PbHAp on the surfaces of CaHAp. The needle-like crystal morphology observed for PbHAp after 24 h reaction time developed into hexagonal-rod crystal morphology within 48 h reaction time. The largest PbHAp crystals obtained from 48 h reaction time have approximate size of $10 \times 10 \times 40$ μm. Powder X-ray diffraction results show mixed phases of CaHAp and PbHAp due to difficulty in separating the PbHAp product from the CaHAp substrate. The PbHAp peaks observed after 24 h of reaction sharpen and increase in intensity after 48 h of reaction confirming that the PbHAp phase is the major product for the 48 h reaction time. EDX results of the crystalline products show high intensity Pb peaks with lead to phosphorous ratio (5 : 3) as expected for PbHAp. Lower intensity Ca peaks are also observed, consistent with incomplete coverage of the CaHAp growth substrate.

1. Introduction

Calcium hydroxyapatite, $Ca_5(PO_4)_3(OH)$, CaHAp, the prototype structure of the apatite series, is the dominant component in biological hard tissues such as bones (about 69 wt% CaHAp) and teeth (about 95 wt% CaHAp) [1]. The structure belongs to space group $P6_3/m$ and is susceptible to ionic substitution in both anion and cation sites. Ca^{2+} can be replaced by various divalent cations including Fe^{2+}, Cr^{2+}, Zn^{2+}, Mg^{2+}, Cd^{2+}, Sr^{2+}, or Pb^{2+} [2–6], PO_4^{3-} can be replaced by AsO_4^{3-} or VO_4^{3-}, and OH^- can be replaced by F^- or Cl^- [7–10].

Complete substitution of Pb^{2+} ions into CaHAp structure results in the isostructural lead hydroxyapatite, sometimes called hydroxypyromorphite, $Pb_5(PO_4)_3(OH)$, PbHAp, which has been studied, including its structure [11, 12] and solubility properties [13], partly because the accumulation of Pb^{2+} in bones accompanies bone diseases. Chronic exposure to lead has been shown to inhibit skeletal development [14] and/or can lead to osteoporosis [15] as the lead localizes in the area of bone formation and resorption, respectively. It is possible that this is a consequence of the lower solubility of PbHAp (pK_{SP} = 62.79) [16] compared to CaHAp (pK_{SP} = 53.28) [17]. Thus, the relationship between CaHAp and PbHAp in terms of their structure and properties as well as their potential interconversions might provide important keys in the understanding of the accumulation of Pb^{2+} in bone.

Studies on the mechanism and phase evolution of Pb^{2+} immobilization by synthetic CaHAp have been reported [18, 19] and show dissolution of CaHAp in Pb^{2+} solution and then concomitant crystallization of PbHAp in the system. The mechanism of PbHAp formation in acidic conditions has been proposed [20, 21] as follows.

Dissolution of CaHAp:

$$Ca_5(PO_4)_3(OH) + 7H^+ \longrightarrow 5Ca^{2+} + 3H_2PO_4^- + H_2O \quad (1)$$

Precipitation of PbHAp:

$$5Pb^{2+} + 3H_2PO_4^- + H_2O \longrightarrow Pb_5(PO_4)_3(OH) + 7H^+ \quad (2)$$

Earlier studies of Pb^{2+} immobilization by hydroxyapatite in the absence of potential substitution ions [22], in the presence of potential substitution anions [23], and in the presence of potential substitution cations [24] show the same dissolution/precipitation mechanism. While the Ca^{2+} and Pb^{2+} compounds are isostructural, they are in separate series due to the difficulty of substituting Pb for Ca in the apatite series or of substituting Ca for Pb in the pyromorphite series [25].

This work reports preparation of CaHAp and its X-ray absorption spectroscopy (XAS) spectrum to characterize the short-range environment around Ca absorbing atoms of the precipitate product. A reflux method was used to increase the CaHAp dissolution rate and thus the PbHAp crystallization rate in the metathesis reaction of CaHAp in lead nitrate solution. The relationship between reaction times and crystal morphologies of products is discussed.

2. Materials and Methods

2.1. Preparation of CaHAp Material. Phosphate and calcium solutions for preparation of CaHAp were prepared by dissolving 7.92 g (60 mmol) diammonium hydrogen phosphate, $(NH_4)_2HPO_4$ (Ajax Finechem, AR grade), in 100 mL deionized water and dissolving 23.60 g (100 mmol) calcium nitrate, $Ca(NO_3)_2{\cdot}4H_2O$ (Ajax Finechem, AR grade), in 100 mL deionized water. CaHAp was prepared by dropwise addition of phosphate solution into calcium solution, while stirring at room temperature and maintaining the solution pH at 11 with 1.0 M NaOH. After addition of the phosphate solution, the suspension was stirred continuously for 30 min and the precipitate was separated by filtration, washed with deionized water three times, and dried at 100°C for 24 h.

2.2. Preparation of PbHAp by Reflux Method. Excess CaHAp, 0.20 g (3.98 mmol), was ground in an agate mortar and added into a solution prepared by dissolving 0.0733 g (0.22 mmol) lead nitrate, $Pb(NO_3)_2$ (Ajax Finechem, AR grade), in 80 mL deionized water and refluxed for 24 h and 48 h. The white precipitates were separated by filtration, washed with deionized water three times, and dried at 100°C for 24 h.

2.3. Characterization. Crystal morphologies were observed by scanning electron microscopy (SEM) using a JSM 6400 electron microscope (JEOL, Japan) equipped with a Microspec model WDX-100 energy dispersive X-ray fluorescence (EDX) detector. IR spectra were acquired on a Perkin-Elmer model Spectrum GX Fourier transform infrared spectrophotometer in wavenumber range 400–4000 cm^{-1} from KBr pellets.

Powder X-ray diffraction (XRD) scans were acquired for the 2θ range 10–55° on a Bruker Analytical X-ray Systems D5005 diffractometer equipped with a Cu Kα sealed tube X-radiation source operating at 40 kV and 40 mA. Comparison with ICDD JCPDS files [26] was utilized for phase identification of products.

X-ray absorption spectroscopy (XAS) experiments were conducted at the BL-8 beamline at the Siam Photon Laboratory of the National Synchrotron Research Center of Thailand (Nakhon Ratchasima, Thailand) with the electron storage ring operated at 1.2 GeV with an average beam current of ~100 mA. A monochromatic beam was obtained by means of a Si(111) double crystal monochromator. Experiments were performed at the Ca K-edge in transmission mode. The gas ionization chamber was filled with N_2 (~400 mbar), and XAS spectra of $CaCl_2{\cdot}2H_2O$ were used for a standard energy calibration (4042 eV). Extended X-ray absorption fine structure, EXAFS, spectra were collected in an energy range between 3970 and 4750 eV, with energy steps of 1 eV. Samples and reference compounds were ground in an agate mortar in air until uniform and were sealed between layers of Kapton tape on the sample holder and then brought to the beam. EXAFS fitting was carried out using the IFEFFIT library [27] within the ATHENA XAS data processing suite [28], and interatomic distance estimates were obtained from the ATHENA suite [29].

3. Results and Discussion

CaHAp structure has been reported [30, 31]. It consists of metal atoms located on two crystallographically different sites: f sites (identified as Ca(I)) and h sites (identified as Ca(II)) as shown in Figure 1. Two metal ions at the Ca(I) sites are coordinated with nine O atoms (six shorter bonds to three O(1) and three O(2) phosphate oxygen atoms on Ca(I) sites define a twisted trigonal prism, and three longer bonds to O(3) atoms extend through the prism faces), and three metal ions at the Ca(II) sites are coordinated with seven O atoms (one O(1), one O(2), and four general O(3) atoms from PO_4^{3-} groups and one O(4) atom from an OH^- group).

EXAFS fitting for CaHAp used the crystallographic parameters for ideally crystalline CaHAp taken from Posner et al. [30]. EXAFS data were Fourier-transformed in the k range 2–10.5 $Å^{-1}$ using k^3-weighting of data and fit in real space in the range of 1–6 Å of the Ca local environment. Figure 2 shows EXAFS of (a) the k^3-weighted raw and fitted χ (chi) functions of the samples and (b) Fourier transformations of k^3-weighted EXAFS spectra. This is the best fit for these available EXAFS spectra. The distances displayed on the x-axis are not corrected for phase shifts and appear offset by about 0.3 Å. The coordination number that is detected by EXAFS spectroscopy is composed of the weighted sum of Ca(I) and Ca(II) sites. Higher shells of light backscattering atoms were omitted due to small intensity, and shells in very close neighborhood were combined in order to keep the number of fit parameters manageable and mathematically significant. Multiple scattering pathways were of negligible magnitude. These results show an average bond distance of all atoms surrounding Ca atoms, Ca–O#1 = 2.41 Å (for Ca–6O), Ca–P#2 = 3.22 Å (Ca–2.4P), Ca–P#3 = 3.59 Å (Ca–2.4P), Ca(I)–Ca(II)#4 = 3.95 Å (Ca–6Ca), Ca(I)–Ca(II)#5 = 4.03 Å (Ca–2.4Ca), and Ca(I)–Ca(I)#6 = 5.45 Å (Ca–3.6Ca).

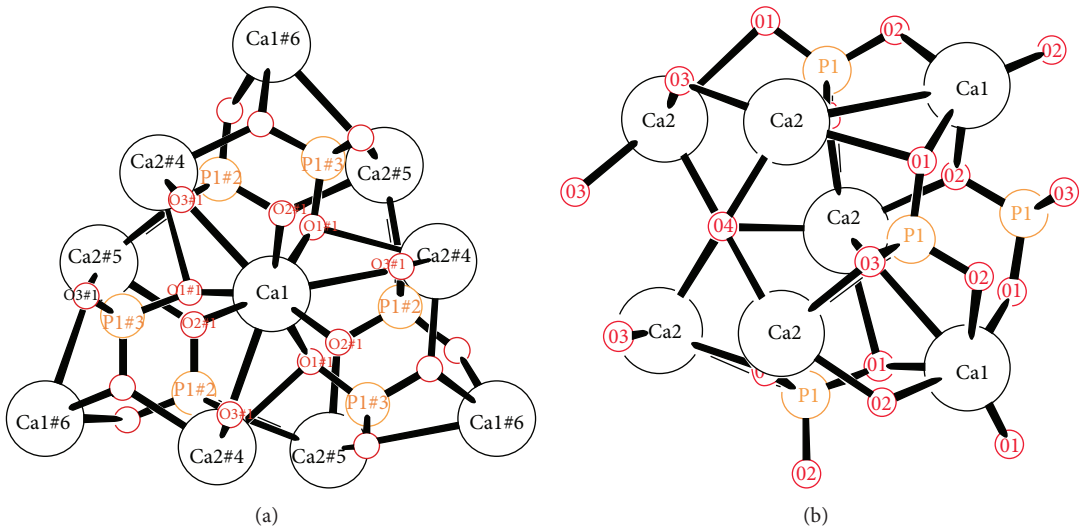

Figure 1: Projection drawings down [001] of (a) Ca(I) site and (b) the Ca(II) site in CaHAp.

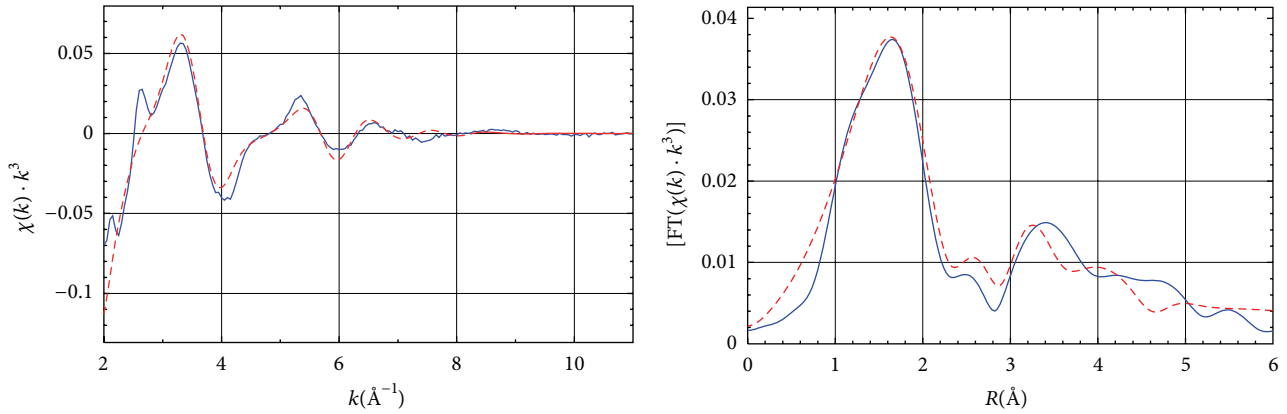

Figure 2: Ca K-edge EXAFS data of CaHAp experiment (solid lines) and fit to data (dashed lines). (a) The k^3-weighted $\chi(k)$ and (b) Fourier transformations of the k^3-weighted EXAFS spectra. Radial distribution functions were not corrected for phase shift (shorter distances by 0.3-0.4 Å with respect to crystallographic values). Note: the dotted lines are best fits.

The SEM images of CaHAp before and after refluxing in lead nitrate solution are shown in Figure 3. Crystalline product after refluxing for 24 h exhibits needle-like crystal morphology on the surface of the CaHAp substrate (Figure 3(b)) while the crystalline product after refluxing for 48 h exhibits hexagonal-rod crystal morphology (Figure 3(c)). The product crystal size increased with increasing reaction time; the largest crystal size observed is about $10 \times 10 \times 40\,\mu$m. The finely divided PbHAp phase could not be easily separated from the CaHAp substrate.

EDX spectra of products and the substrate after refluxing in lead nitrate solution are shown in Figure 4. The EDX spectrum of the post reaction CaHAp substrate (Figure 4(a)) shows high intensity Ca peaks with calcium to phosphorous ratio of about 5 : 3 as expected for CaHAp (but no evidence of Pb peaks), while the spectrum of crystalline product region (Figure 4(b)) shows high intensity Pb peaks with lead to phosphorous ratio of 5 : 3 as expected for PbHAp. Low intensity Ca peaks are also observed in the product spectra, consistent with incomplete coverage of the CaHAp growth substrate. Similar spectra (not shown) were observed for the CaHAp substrate and PbHAp product areas after refluxing for 48 h. These spectra support the dissolution/precipitation mechanism previously proposed [20, 21] and do not give any suggestion of substitution of Ca^{2+} by Pb^{2+} in the CaHAp substrate to form a solid solution under the mild conditions of refluxing in H_2O.

XRD patterns of products after refluxing for 24 h and 48 h also show mixed PbHAp (JCPDS number 08-0259) and CaHAp (JCPDS number 09-0432) phases as shown in Figure 5.

The XRD pattern of the product after 48 h reflux clearly shows the PbHAp phase as the major product phase with the intensity of PbHAp peaks considerably increased, indicating

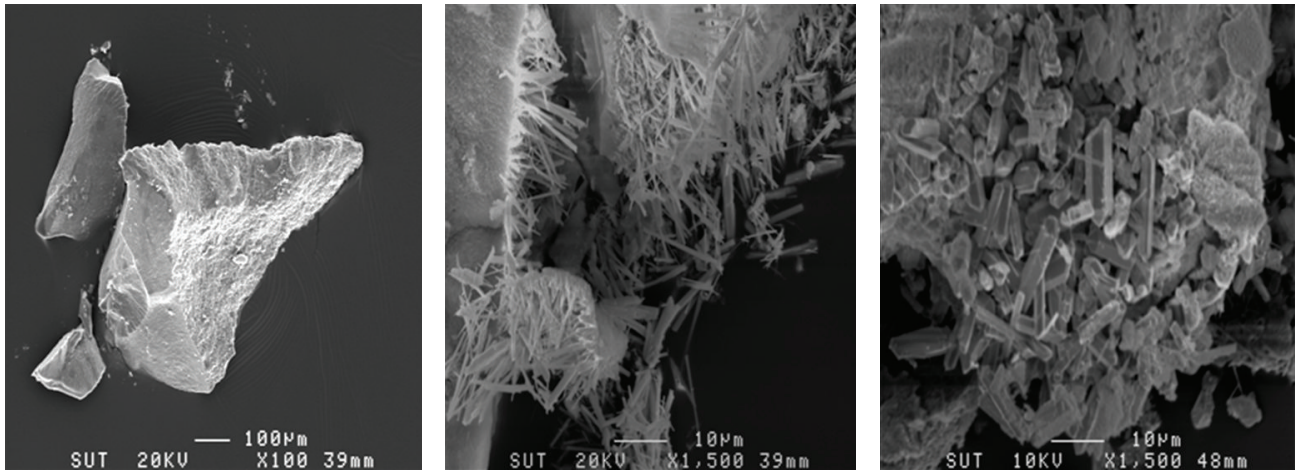

(a) (b) (c)

Figure 3: SEM images of (a) CaHAp before refluxing, (b) after refluxing in lead nitrate solution (917 mg/L) for 24 h, and (c) after refluxing for 48 h.

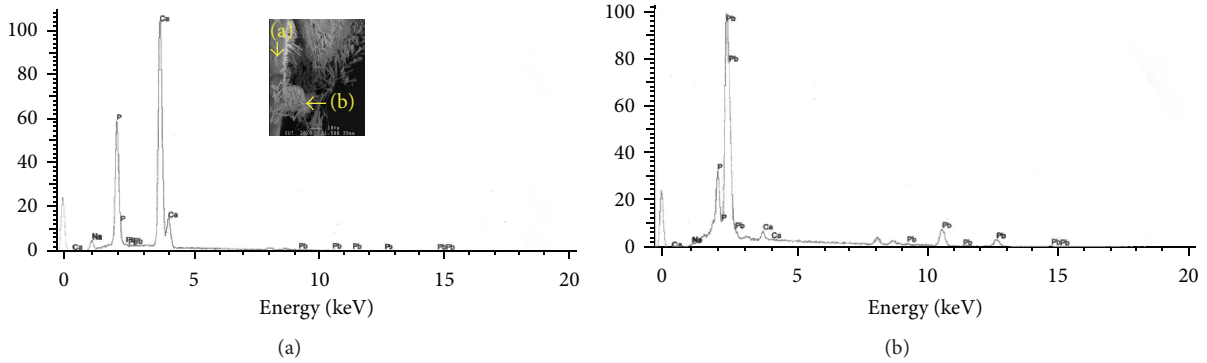

Figure 4: EDX spectra of products after refluxing in lead nitrate solution (917 mg/L) for 24 h. (a) CaHAp substrate and (b) PbHAp needle-like crystal product region. The inset shows the locations sampled for the spectra.

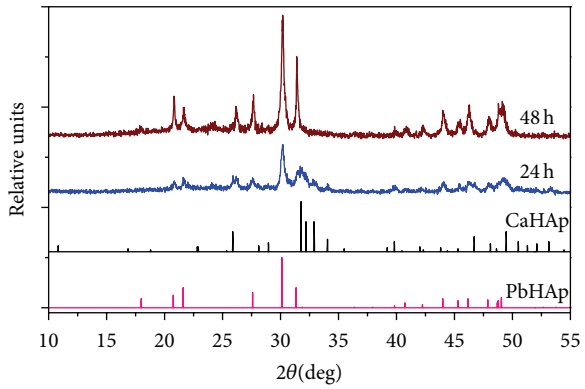

Figure 5: XRD patterns of products after refluxing in lead nitrate solution (917 mg/L) for 24 h and 48 h.

that formation of PbHAp phase increased with increased reaction time which is in agreement with previous work [18]. PbHAp crystal product is present as hexagonal rod-shaped crystals as shown in Figure 3(c). The presence of both phases results from difficulty separating the finely divided PbHAp phase from the approximately 20-fold excess CaHAp reactant substrate phase.

IR spectra of CaHAp and products after refluxing in the presence of Pb^{+2} (Figure 6) show bands in the appropriate regions: $\upsilon_{1(P-O)}$ and $\upsilon_{3(P-O)}$ PO_4^{3-} stretching modes in the 961–1095 cm^{-1} region, $\upsilon_{2(O-P-O)}$ bending mode in the 467–473 cm^{-1} region, and the $\upsilon_{4(O-P-O)}$ bending mode in the 562–632 cm^{-1} region, consistent with previous reports for CaHAp [32, 33] and PbHAp [34].

The CaHAp reactant material was not calcined and shows broad water O–H stretching vibrational bands centered about 3468 cm^{-1} in the CaHAp spectrum with the ν_{OH} apatite band as a shoulder at 3568 cm^{-1}, similar to reported values of 3573 [32] and 3569 cm^{-1} [33]. A small sharp O–H stretching mode appears at 3571 cm^{-1} in the product spectra, which compares favorably with the apatite bands and the reported [34] ν_{OH} vibrational stretching band for pure PbHAp at 3560 cm^{-1}. A broad band in the 3000–3700 cm^{-1} region and a weak

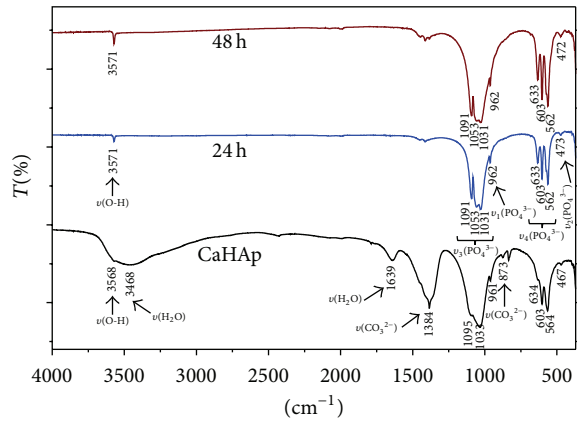

FIGURE 6: IR spectra of CaHAp before refluxing and after refluxing in lead nitrate solution (917 mg/L) for 24 h and 48 h.

peak at 1639 cm^{-1} in the CaHAp spectrum are consistent with absorbed H_2O on the KBr pellet or associated with the reactant substrate phase. As all the IR spectroscopy samples were prepared in the same manner, loss of these broad peaks on refluxing indicates that they are due to water associated with the reactant substrate phase.

The IR spectrum of CaHAp also shows bands of CO_3^{2-} stretching at 1384 cm^{-1} and CO_3^{2-} bending at 873 cm^{-1} in agreement with previous work [35]. The carbonate may come from the incorporation of atmospheric CO_2 through equilibrium with the alkaline reaction solution during the synthesis step. The incorporation of CO_3^{2-} into CaHAp materials has been suggested to increase the solubility of CaHAp [36].

4. Conclusion

The reflux method of CaHAp dissolution to provide phosphate anion in the presence of lead cation succeeds for producing larger sized crystals of the less soluble PbHAp from the aqueous solution. Hexagonal rod-shaped crystals of PbHAp formed and product crystal size increased with increasing reflux-reaction time. EDX results are consistent with the XRD results and show mixed phases of PbHAp and substrate CaHAp, but no evidence of Pb substitution into the CaHAp substrate phase. IR results indicate the incorporation of carbonate in the CaHAp substrate resulting in increased solubility of this material, but the carbonate anion does not appear to carry over into the PbHAp product crystals.

Conflict of Interests

The authors declare that there is no conflict of interests regarding the publication of this paper.

References

[1] R. Z. LeGeros, *Calcium Phosphates in Oral Biology and Medicine*, Karger, San Francisco, Calif, USA, 1st edition, 1991.

[2] T. Moriguchil, S. Nakagawa, and F. Kaji, "Reaction of Ca-deficient hydroxyapatite with heavy metal ions along with metal substitution," *Phosphorus Research Bulletin*, vol. 22, pp. 54–60, 2008.

[3] A. Yasukawa, T. Yokoyama, K. Kandori, and T. Ishikawa, "Reaction of calcium hydroxyapatite with Cd^{2+} and Pb^{2+} ions," *Colloids and Surfaces A*, vol. 299, no. 1–3, pp. 203–208, 2007.

[4] F. Ren, Y. Leng, R. Xin, and X. Ge, "Synthesis, characterization and ab initio simulation of magnesium-substituted hydroxyapatite," *Acta Biomaterialia*, vol. 6, no. 7, pp. 2787–2796, 2010.

[5] M. D. O'Donnell, Y. Fredholm, A. de Rouffignac, and R. G. Hill, "Structural analysis of a series of strontium-substituted apatites," *Acta Biomaterialia*, vol. 4, no. 5, pp. 1455–1464, 2008.

[6] H. Xu, L. Yang, P. Wang, Y. Liu, and M. Peng, "Removal mechanism of aqueous lead by a novel eco-material: carbonate hydroxyapatite," *Journal of Materials Science and Technology*, vol. 23, no. 3, pp. 417–422, 2007.

[7] Z. Dong, T. J. White, B. Wei, and K. Laursen, "Model apatite systems for the stabilization of toxic metals: I, calcium lead vanadate," *Journal of the American Ceramic Society*, vol. 85, no. 10, pp. 2515–2522, 2002.

[8] Y. Dai and M. J. Hughes, "Crystal structure refinements of vanadinite and pyromorphite," *Canadian Mineralogist*, vol. 27, pp. 189–192, 1989.

[9] W. Dungkaew, K. J. Haller, A. E. Flood, and J. F. Scamehorn, "Arsenic removal by precipitation with Calcium phosphate hydroxyapatite," *Advanced Materials Research*, vol. 506, pp. 413–416, 2012.

[10] T. Dordević, S. Šutović, J. Stojanović, and L. Karanović, "Sr, Ba and Cd arsenates with the apatite-type structure," *Acta Crystallographica C*, vol. 64, pp. i82–i86, 2008.

[11] S. Brückner, G. Lusvardi, L. Menabue, and M. Saladini, "Crystal structure of lead hydroxyapatite from powder X-ray diffraction data," *Inorganica Chimica Acta*, vol. 236, no. 1-2, pp. 209–212, 1995.

[12] J. Y. Kim, R. R. Fenton, B. A. Hunter, and B. J. Kennedy, "Powder diffraction studies of synthetic calcium and lead apatites," *Australian Journal of Chemistry*, vol. 53, no. 8, pp. 679–686, 2000.

[13] E. Valsami-Jones, K. V. Ragnarsdottir, A. Putnis, D. Bosbach, A. J. Kemp, and G. Cressey, "The dissolution of apatite in the presence of aqueous metal cations at pH 2-7," *Chemical Geology*, vol. 151, no. 1–4, pp. 215–233, 1998.

[14] J. D. Hamilton and E. J. O'Flaherty, "Influence of lead on mineralization during bone growth," *Fundamental and Applied Toxicology*, vol. 26, no. 2, pp. 265–271, 1995.

[15] H. E. Gruber, H. C. Gonick, F. Khalil-Manesh et al., "Osteopenia induced by long-term, low- and high-level exposure of the adult rat to lead," *Mineral and Electrolyte Metabolism*, vol. 23, no. 2, pp. 65–73, 1997.

[16] D. L. Parkhurst and C. A. J. Appelo, "PHREEQC (version 2) A computer program for speciation, batch-reaction, one-dimensional transport, and inverse geochemical calculations," U.S. Department of the Interior and U.S. Geological Survey, http://pfw.antipodes.nl/download.html, The minteq.v4.dat database accessed with the PHREEQC software, 1999, http://www.phreeplot.org/ppihtml/minteq.v4.dat.html.

[17] Y. Zhu, X. Zhang, Y. Chen et al., "A comparative study on the dissolution and solubility of hydroxylapatite and fluorapatite at 25°C and 45°C," *Chemical Geology*, vol. 268, no. 1-2, pp. 89–96, 2009.

[18] E. Mavropoulos, A. M. Rossi, A. M. Costa, C. A. C. Perez, J. C. Moreira, and M. Saldanha, "Studies on the mechanisms of lead immobilization by hydroxyapatite," *Environmental Science & Technology*, vol. 36, no. 7, pp. 1625–1629, 2002.

[19] E. Mavropoulos, N. C. C. Rocha, J. C. Moreira, A. M. Rossi, and G. A. Soares, "Characterization of phase evolution during lead immobilization by synthetic hydroxyapatite," *Materials Characterization*, vol. 53, no. 1, pp. 71–78, 2004.

[20] W. L. Lindsay, *Chemical Equilibria in Soils*, John Wiley & Sons, New York, NY, USA, 1979.

[21] L. Dong, Z. Zhu, Y. Qiu, and J. Zhao, "Removal of lead from aqueous solution by hydroxyapatite/magnetite composite adsorbent," *Chemical Engineering Journal*, vol. 165, no. 3, pp. 827–834, 2010.

[22] Q. Y. Ma, S. J. Traina, T. J. Logan, and J. A. Ryan, "In situ lead immobilization by apatite," *Environmental Science & Technology*, vol. 27, no. 9, pp. 1803–1810, 1993.

[23] Q. Y. M. Qi Ying Ma, S. J. Tralna, T. J. Logan, and J. A. Ryan, "Effects of aqueous Al, Cd, Cu, Fe(II), Ni, and Zn on Pb immobilization by hydroxyapatite," *Environmental Science & Technology*, vol. 28, no. 7, pp. 1219–1228, 1994.

[24] Q. Y. Ma, S. J. Traina, T. J. Logan, and J. A. Ryan, "Effects of NO_3^-, Cl^-, F^-, SO_4^{2-}, CO_3^{2-} on Pb2+ immobilization by hydroxyapatite," *Environmental Science & Technology*, vol. 28, pp. 408–418, 1994.

[25] J. R. van Wazer, *Phosphorus and Its Compounds*, Interscience, New York, NY, USA, 1958.

[26] ICDD, *Powder Diffraction Files (Database)*, International Center for Diffraction Data, Newtown Square, Pa, USA, 2007.

[27] M. Newville, "IFEFFIT: interactive XAFS analysis and FEFF fitting," *Journal of Synchrotron Radiation*, vol. 8, no. 2, pp. 322–324, 2001.

[28] B. Ravel and M. Newville, "ATHENA, ARTEMIS, HEPHAESTUS: data analysis for X-ray absorption spectroscopy using IFEFFIT," *Journal of Synchrotron Radiation*, vol. 12, no. 4, pp. 537–541, 2005.

[29] B. Ravel, *ATHENA User's Guide*, University of Chicago, 2009.

[30] A. S. Posner, A. Perloff, and A. F. Diorio, "Refinement of the hydroxyapatite structure," *Acta Crystallographica*, vol. 11, pp. 308–309, 1958.

[31] M. I. Kay, R. A. Young, and A. S. Posner, "Crystal structure of hydroxyapatite," *Nature*, vol. 204, no. 4963, pp. 1050–1052, 1964.

[32] M. Jevtić, M. Mitrić, S. Škapin, B. Jančar, N. Ignjatović, and D. Uskoković, "Crystal structure of hydroxyapatite nanorods synthesized by sonochemical homogeneous precipitation," *Crystal Growth and Design*, vol. 8, no. 7, pp. 2217–2222, 2008.

[33] S. Lazarević, I. Janković-Častvan, D. Tanasković, V. Pavićević, D. Janaćković, and R. Petrović, "Sorption of Pb^{2+}, Cd^{2+}, and Sr^{2+} ions on calcium hydroxyapatite powder obtained by the hydrothermal method," *Journal of Environmental Engineering*, vol. 134, pp. 683–688, 2008.

[34] V. Laperche and S. J. Traina, "Immobilization of Pb by hydroxyapatite," in *Adsorption of Metals By Geomedia*, E. A. Jenne, Ed., pp. 255–277, Academic Press, San Diego, Calif, USA, 1998.

[35] S. M. Barinov, I. V. Fadeeva, D. Ferro et al., "Stabilization of carbonate hydroxyapatite by isomorphic substitutions of sodium for calcium," *Russian Journal of Inorganic Chemistry*, vol. 53, no. 2, pp. 164–168, 2008.

[36] S. Liao, F. Watari, G. Xu, M. Ngiam, S. Ramakrishna, and C. K. Chan, "Morphological effects of variant carbonates in biomimetic hydroxyapatite," *Materials Letters*, vol. 61, no. 17, pp. 3624–3628, 2007.